Earth Surface Processes and Landforms
Earth Surf. Process. Landforms **30**, 1051–1067 (2005)
Published online in Wiley InterScience (www.interscience.wiley.com). **DOI:** 10.1002/esp.1262

Measuring middle Pleistocene erosion rates with cosmic-ray-produced nuclides in buried alluvial sediment, Fisher Valley, southeastern Utah

Greg Balco* and John O. H. Stone
Quaternary Research Center and Department of Earth and Space Sciences, University of Washington, Seattle, WA 98195-1310, USA

**Correspondence to: G. Balco, Quaternary Research Center and Department of Earth and Space Sciences, University of Washington, Seattle, WA 98195-1310, USA. E-mail: balcs@u.washington.edu*

Abstract

Cosmic-ray-produced ^{10}Be and ^{26}Al in riverborne quartz sediment are commonly used to estimate average catchment-scale erosion rates. Likewise, the concentrations of these nuclides in ancient sediments, stored in a depositional basin, carry a record of past erosion rates in the sediment source area. This is important because such a record could be compared to records of climate change or tectonic events to elucidate relationships between climate, tectonics and erosion. If the sediments are shielded from the cosmic-ray flux after deposition, for example in deep water, their nuclide concentrations need only be corrected for radioactive decay since deposition in order to determine past erosion rates. Where sediment is deposited subaerially and buried relatively slowly, on the other hand, the additional nuclide concentration that builds up during sediment accumulation and storage must be reconstructed and subtracted in order to recover the initial nuclide concentrations in the sediment and thence the past erosion rates. We describe an example of this process for an early to middle Pleistocene section of alluvial sediment in Fisher Valley, Utah. We use stratigraphic observations as well as an independently known age model for the sediment section to: (a) subtract post-depositional nuclide concentrations and reconstruct past erosion rates between 0·7 and 0·6 Ma; and (b) estimate the uncertainty in the results that arises from imperfect dating of the section and the natural variability in accumulation rates. The present basin-averaged erosion rate in Fisher Valley is near 125 m Ma^{-1}, and middle Pleistocene basin-averaged erosion rates varied between 80 and 220 m Ma^{-1}. Changes in the erosion rate over time do not appear to be connected to glacial–interglacial climate changes, but may be related to episodic subsidence of the basin. Uncertainties are small in the case of low erosion rates and high sediment accumulation rates, and large in the opposite situation. In this example, we could reduce the uncertainties by increasing the sampling density or by better relating our sample locations to the small-scale stratigraphy of the sedimentary section. In general, future attempts to reconstruct past erosion rates from cosmogenic-nuclide concentrations in ancient alluvium will be most successful in situations where post-depositional nuclide accumulation is minimized, for example in lakes or marine basins. Copyright © 2005 John Wiley & Sons, Ltd.

Received 1 September 2004;
Revised 28 February 2005;
Accepted 17 March 2005

Keywords: middle Pleistocene; Utah; Colorado Plateau; erosion rates; cosmogenic nuclides

Introduction

In this paper we describe how measurements of the cosmic-ray-produced radionuclides ^{10}Be and ^{26}Al in alluvial sediment can be used to develop a continuous record of erosion rate changes through time. Records of past changes in erosion rates are important because erosion is the key link by which climate can affect tectonic processes as well as an important internal feedback in orogenic development. In order to fully understand the climate–erosion–tectonics feedback system, it is necessary to separately understand the relationships between climate and erosion rate and between tectonic regime and erosion rate (e.g. Molnar, 2003). A number of studies have sought to establish these relationships by measuring erosion or exhumation rates in areas subject to different climates and tectonic regimes,

for example, by sediment yield measurements (e.g. Langbein and Schumm, 1958; Schumm and Hadley, 1961), thermochronology (e.g. Reiners *et al*., 2003), or cosmogenic-nuclide geochemistry (e.g. Riebe *et al*., 2001).

Ergodic approaches to climate–tectonics–erosion studies

The results of these studies of the spatial variability of erosion rates vary widely (e.g. Molnar, 2003), showing that the relation of either climate or tectonics to erosion rates varies in different settings, and it is not our purpose here to review these studies in detail. The important aspect of this work from our perspective is that the study of the relationship between climate, tectonics, and erosion in general was originally motivated by questions about the effect of *changes* in climate or tectonics over time on erosion rates (e.g. Molnar and England, 1990; Raymo and Ruddiman, 1992). However, using spatial relationships between climate or tectonics and erosion, to evaluate hypotheses about temporal changes in erosion rates in response to climatic or tectonic forcing, requires two important assumptions. The first assumption is that erosion rates in the modern landscapes being observed are fully adjusted to and in equilibrium with the climatic or tectonic forcing factors of interest (an equilibrium assumption). The second is that the difference in present erosion rates under two different climates is the same as the change in erosion rates that would occur if the climate changed from one state to the other (an actualist, or ergodic, assumption).

Neither of these assumptions is likely to be universally, or even commonly, true. First, the details of equilibrium assumptions, and the timescales over which they must apply, vary among methods for measuring erosion rates, but in all cases, if erosion is unsteady on a timescale which invalidates the assumptions of one of these methods, then the results of a spatial study of erosion rates may be entirely wrong or severely biased. Second, the ergodic assumption fails if the rate of change, or the frequency of change, in the forcing factors is as important as their state in determining the erosional response (e.g. Schumm and Rea, 1995). A landscape that is never allowed to equilibrate completely with either one or another climate state may evolve faster than one which is allowed to fully equilibrate with either of the two states. A study of landscapes currently in the two end-member states could never capture this effect. Thus, the approach of swapping spatial for temporal variability in erosion rates and their forcing factors is not entirely adequate to answer questions about the effects of temporal changes in climate or tectonics on erosion rates.

Records of erosion rate changes through time

The obvious way to address the challenge of distinguishing the effect of different climatic or tectonic regimes on erosion rates from the effect of the change between those regimes, as well as the challenge of evaluating the steady-state assumptions usually needed to measure erosion rates at all, is to develop records of erosion rate changes through time. This is difficult, because any eroding landscape inherently removes the evidence of its former configuration. In the past, the only means of doing this has been by serial sediment mass-balance. For example, Pazzaglia and Brandon (1996) compiled sediment thickness measurements in the western Atlantic Ocean to establish the denudation history of the Appalachians over the last 175 Ma, and Collier *et al*. (2000) took advantage of the closed basin of the Gulf of Corinth in Greece to show that erosion rates in the surrounding uplands were much greater during the last glacial maximum than during the Holocene. Mass-balance measurements of erosion rates such as these are potentially very accurate, but are limited to fortuitous geological circumstances where a closed basin is associated with a fixed drainage area, and there exist accurately dated stratigraphic markers that may be used to assign sediment to different time periods. Thus, the resolution of such erosion rate records is generally much lower than that of comparable climate records, which makes it difficult to compare the two (although Koppes and Hallet (2002) report a creative example that overcomes this limitation).

In this paper we discuss a different method of developing records of erosion rate changes through time that is based on the cosmic-ray-produced radionuclides ^{10}Be and ^{26}Al. These nuclides are produced within mineral grains during cosmic-ray bombardment of surface rocks and sediments. Most cosmic rays stop within a few metres of the Earth's surface, so the nuclide concentration in sediment shed from an eroding surface is proportional to the length of time that the sediment spent in the upper few metres, which in turn is inversely proportional to the erosion rate. Likewise, the nuclide concentration in river sediment reflects the average erosion rate in the drainage basin upstream (e.g. Lal, 1991; Cerling and Craig, 1994; Bierman and Steig, 1996; Brown *et al*., 1995; Granger *et al*., 1996; Bierman and Nichols, 2004). When this sediment is transported to a depositional basin and stored, it forms a record of past erosion rates. This idea offers two improvements on the mass-balance method of measuring past erosion rates. First, it requires only a small sample, and not the entire inventory, of the sediment that left the basin during a particular time period. Second, it requires only an age model for a single sedimentary section with no need for age correlations over entire basins. Thus, it can in priniciple be applied in a much wider variety of geological situations, and can potentially yield much higher-resolution records of past erosion rates than mass-balance methods. It is similar in principle to the idea of

measuring changes in past exhumation rates by thermochronology of detrital sediments shed from an eroding mountain belt and preserved in foreland basins (Garver *et al*., 1999). The cooling ages of mineral grains eroding at the surface, however, reflect the integrated erosion rates over the millions of years needed to exhume these grains from depths of several kilometres; the cosmogenic-nuclide concentration in detrital sediment integrates only the time required for 1–2 m of surface lowering and can provide a much higher-resolution record.

The idea of inferring past erosion rates from cosmogenic-nuclide concentrations in ancient alluvial sediment has been applied twice before, first by Granger *et al*. (1997, 2001) who determined past erosion rates in basins in the central USA as a byproduct of dating fluvial sediments stranded in caves by ^{26}Al-^{10}Be 'burial dating', and second by Schaller *et al*. (2002, 2004), who measured ^{10}Be concentrations in sediment from fluvial terraces of the Meuse and Loire rivers and inferred a discontinuous record of erosion rates over the last 1·3 million years. Although these studies provided new and fundamentally important information about past erosion rates, they were limited by the episodic nature of cave and terrace formation, and the fact that terraces are most likely to be emplaced only during a certain type of climate transition. In this paper, we discuss how the same idea can be applied to continuous sections of alluvial sediment, to potentially yield records of erosion rate changes with higher resolution and better continuity. We illustrate the method, and evaluate its uncertainty and thus usefulness in realistic situations, with an example from a middle Pleistocene alluvial section in Fisher Valley, Utah. Finally, we suggest how it might best be employed in future to answer questions about the relationship of climate, tectonics, and landscape evolution.

Inferring Past Erosion Rates from Cosmogenic-Nuclide Concentrations in Sediment

The concentration of ^{10}Be or ^{26}Al in alluvial sediment leaving a steadily eroding catchment area is inversely proportional to the erosion rate in the catchment, as follows:

$$N_{i,E} = \frac{\Lambda \bar{P}_i}{\rho \bar{\varepsilon}} \tag{1}$$

where $N_{i,E}$ is the concentration of nuclide i developed during erosion of the sediment (atoms g^{-1}), Λ is the effective attenuation length for spallation (160 g cm^{-2}), $\bar{P}_i$ is the mean production rate of nuclide i in the catchment (atoms g^{-1} a^{-1}), ρ is the density of the eroding material (g cm^{-3}), and $\bar{\varepsilon}$ is the mean erosion rate in the catchment (cm a^{-1}). There are several assumptions inherent in this formula: we discuss some of them below, and Bierman and Steig (1996), Brown *et al*. (1995) and Granger *et al*. (1996) provide a more detailed discussion as well as a complete derivation of the formula. Other authors (e.g. Schaller *et al*., 2004) use a more complicated version of Equation 1 which accounts for subsurface nuclide production by muons; we retain the simple form for clarity and because we are less interested in making precise erosion rate estimates than in identifying changes in erosion rates.

We are interested in recovering the nuclide concentration attributable to erosion $N_{i,E}$, and thence the past erosion rate, from sediment that has left the catchment area we are interested in and then been stored in a sedimentary deposit. The nuclide concentration in a sample of such sediment is:

$$N_i = N_{i,E} e^{-\lambda_i t_D} + N_{i,D} \tag{2}$$

where N_i is the measured concentration of nuclide i in the sample at the present time (atoms g^{-1}), t_D is the time since sediment deposition (a), λ_i is the decay constant of nuclide i ($\lambda_{10} = 4{\cdot}62 \times 10^{-7}$ a^{-1}; $\lambda_{26} = 9{\cdot}89 \times 10^{-7}$ a^{-1}), and $N_{i,D}$ is the nuclide concentration attributable to nuclide production during deposition and subsequent storage (atoms g^{-1}). The erosional nuclide concentration $N_{i,E}$ reflects all the atoms that were present in the sediment *at the time it was deposited*, and the depositional nuclide concentration $N_{i,D}$ reflects all the atoms in the sediment that were produced *after the sediment was deposited*.

The most important implication of Equation 2 is that the simplest way to determine the erosional nuclide concentration $N_{i,E}$ from the measured nuclide concentration N_i would be to collect sediment that was transported directly from an eroding catchment to the bottom of a lake, or the ocean, where the cosmic ray flux is near zero. In this case $N_{i,D}$ would be near zero as well. This is important because the need to estimate $N_{i,E}$ and $N_{i,D}$ separately is the major obstacle to obtaining continuous records of past erosion rates by this technique: if $N_{i,D}$ were assured to be zero the technique would be much more powerful, and most of the complications that we describe later in this paper could be ignored. However, collecting lacustrine or marine sediment presents a variety of new problems: the need to understand transport paths in detail to ensure that sediment can be directly connected to its source area; the expense of collecting

sediment cores in deep water; and the difficulty of obtaining large samples of sand-sized quartz from sediment cores. This last difficulty arises because it is difficult to reliably prepare pure quartz separates, which are necessary for ^{26}Al and ^{10}Be extraction, from sediment smaller than 100 μm, but most lacustrine and marine coring programmes have been designed to sample silt- and clay-sized sediment. We emphasize that this technique would be most accurate, and therefore most useful, if applied to deep-water sediments, but actually achieving this will require coring sites and practices different from those usually used for palaeoclimate studies.

In this paper, therefore, we discuss how to determine $N_{i,E}$ when $N_{i,D}$ is not zero. This is the case for sediment that was only shallowly buried after it was deposited, that is, most sediment deposited above water. The basic approach is as follows. If we know the age of the sedimentary deposit and the rate at which it accumulated, then we know the burial depth of a particular sediment sample at any time since deposition, that is, the function $z(t)$ where z is the sample depth. If we also know the depth-dependence of nuclide production rates $P_i(z)$, then we can calculate $N_{i,D}$ by solving:

$$\frac{dN_{i,D}}{dt} = P_i(z(t)) - \lambda_i N_{i,D} \tag{3}$$

for each nuclide in each sample, on the domain $t \in [0,t_D]$ where $t = 0$ at the time the sediment sample was deposited and $t = t_D$ at the present time. Knowing t_D and $N_{i,D}$, we can then use Equation 2 to calculate $N_{i,E}$ and Equation 1 to calculate $\bar{\varepsilon}$. For example, Schaller *et al*. (2002, 2004) calculated past erosion rates from sand preserved in fluvial terraces of known age by measuring ^{10}Be concentrations in the sand, then computing $N_{i,D}$ by assuming that the terrace was deposited instantaneously and the sample resided at its present depth since terrace emplacement. In this paper, we face the additional challenge that our sediments were gradually deposited over a long period of time, and the function $z(t)$ is therefore much more complicated.

There are some additional assumptions which are important for inferring either present or past erosion rates from sediment samples. First, both Equations 1 and 2 assume that sediment transport from source to sink is instantaneous with respect to nuclide accumulation. In a situation where a small drainage basin drained by a bedrock-floored stream is immediately adjacent to the depositional basin (such as the example from Fisher Valley that we describe below), this assumption is reasonable. In larger river systems with significant sediment accumulations in the floodplain or in alluvial terraces, sediment storage and recycling between the erosional and depositional parts of the system would violate this assumption. Second, we must know the source drainage area of the sample, otherwise we could not calculate the production rate $\bar{P}$. Third, there must be no recycling or mixing of sediment of different ages. Fourth, the sediment must contain sand-sized quartz to allow measurement of nuclide concentrations at all. Finally, as noted above, Equation 1 also includes some other assumptions regarding the spatial and temporal uniformity of erosion and sediment transport; these are discussed at length elsewhere (e.g. Bierman and Nichols, 2004) and are not the focus of this study.

One aspect of Equation 1 which is important for our purposes, however, concerns the averaging time of the erosion rate that can be inferred from a sample of stream sediment. The nuclide concentration in this sediment reflects exposure during the entire period of time in which the sample traversed the upper few metres below the surface; thus, the time required for the nuclide concentration in sediment to equilibrate with a new erosion rate depends on the erosion rate itself, and is approximately the time required to remove 1–2 m of material. This characteristic averaging time is a fundamental limitation on the timescale of erosion rate changes that can be captured by this technique. Bierman and Steig (1996) and Schaller *et al*. (2004) discuss this in more detail. In this study, we are concerned with erosion rates of approximately 100–200 μm a^{-1}, which means that the characteristic averaging time of our erosion rate measurements is 5000–10 000 years.

Example from Fisher Valley, Utah

Geological setting of the Fisher Valley section

At Fisher Valley, near the town of Moab, Utah, an anticlinal valley cored by a salt diapir preserves a thick section of alluvial sediments deposited between 0·25 and 2·5 Ma (Figures 1–6). The sediments are derived from the erosion of Permian to Jurassic sandstones and siltstones exposed at higher elevations on the north side of the La Sal Mountains (Figure 3), and are composed of fluvial sand and gravel with minor aeolian sand. At *c*. 2·5 Ma, extrusion of the Onion Creek salt diapir into the west end of Fisher Valley caused uplift of the western end of Fisher Creek, creating accommodation space for sediment eroded from its headwaters. Sediment accumulated steadily until *c*. 0·25 Ma, at which point the valley had been filled sufficiently for Cottonwood Creek to capture the headwaters of Fisher Creek

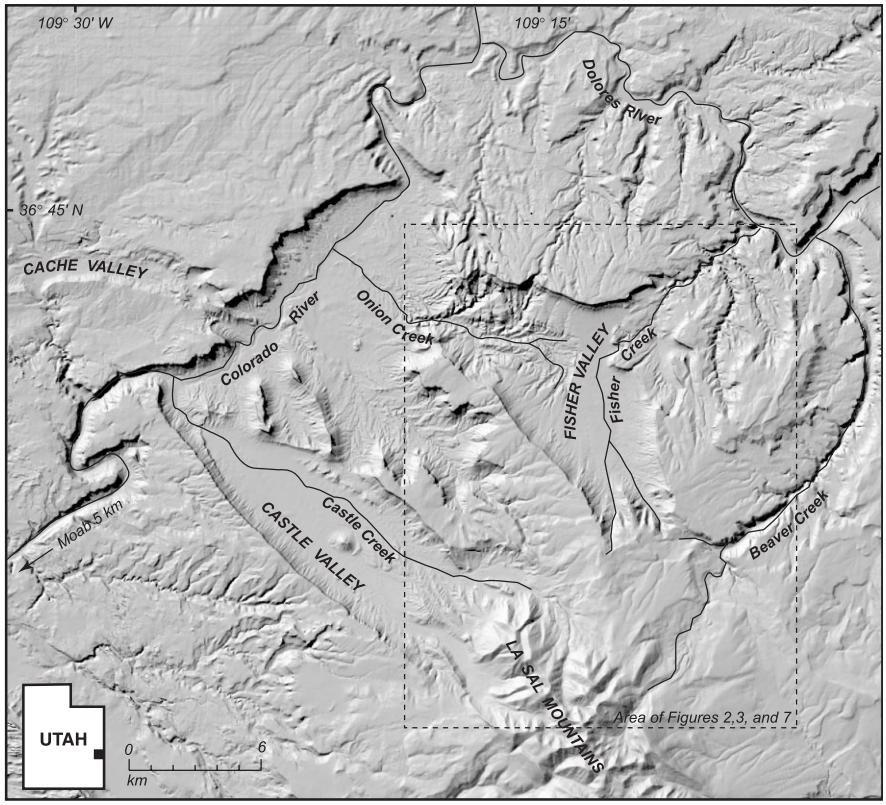

Figure 1. Location of Fisher Valley. Adapted from Colman (1986b).

and divert valley drainage to the northeast. Sediment accumulation stopped at this time. Since then, extrusion of the Onion Creek diapir has apparently slowed, and headward erosion by the remaining lower part of Onion Creek has very rapidly exhumed the western portion of the alluvial section (Figure 2). Shoemaker (1954), Colman (1983), Colman and Hawkins (1985) and Colman *et al.* (1986a,b) describe the stratigraphy and geological history of Fisher Valley in detail. For our purposes, the important features of the geomorphic setting are as follows. First, Colman (1983) investigated the provenance of clasts throughout the alluvial section and concluded that the drainage basin that the sediments were derived from has been the same as the present drainage area since the early Pleistocene. Second, the sediments consist nearly entirely of quartz sand and gravel. Third, the early Pleistocene to present drainage basin does not include glaciated parts of the La Sal Mountains. Fourth, the age of the sediments has been established by a variety of dating methods (Colman *et al*., 1986a; see detailed discussion below).

The alluvial sediments themselves consist of calcic palaeosols, which reflect relative surface stability and low rates of sediment accumulation, intercalated with unweathered sands and gravels that reflect rapid sediment accumulation in a braided-stream environment (Figure 6). Colman *et al.* (1986b) describe the alluvial stratigraphy and the soil properties in detail. Three aspects of the stratigraphy are important in the context of this work. First, with the exception of minor aeolian fine sand units, fine-grained sediments are absent, indicating that ancestral Fisher Creek was never impounded sufficiently to form a lake upstream of the diapir, but continually transported sediment through the basin and out into the Colorado River. This is important because it means that the basin was never closed, and we cannot infer upstream erosion rates from the volume of alluvial sediment in the basin. Second, the age and number of palaeosols in the middle and upper Pleistocene parts of the section indicate that the soils formed during major interglacial periods. Near the centre of the basin, the sediment section is conformable, indicating continuous deposition with periods of slow sediment accumulation, but no significant erosion, during interglaciations. Third, there are at least four angular unconformities in the alluvial deposits near the edges of the basin, suggesting periods of enhanced subsidence of the basin relative to the diapir at its mouth.

To summarize, the alluvial deposits in Fisher Valley record changes in sediment supply, sediment trapping efficiency, or both, that were very likely related to either climate (suggested by the association of palaeosols with

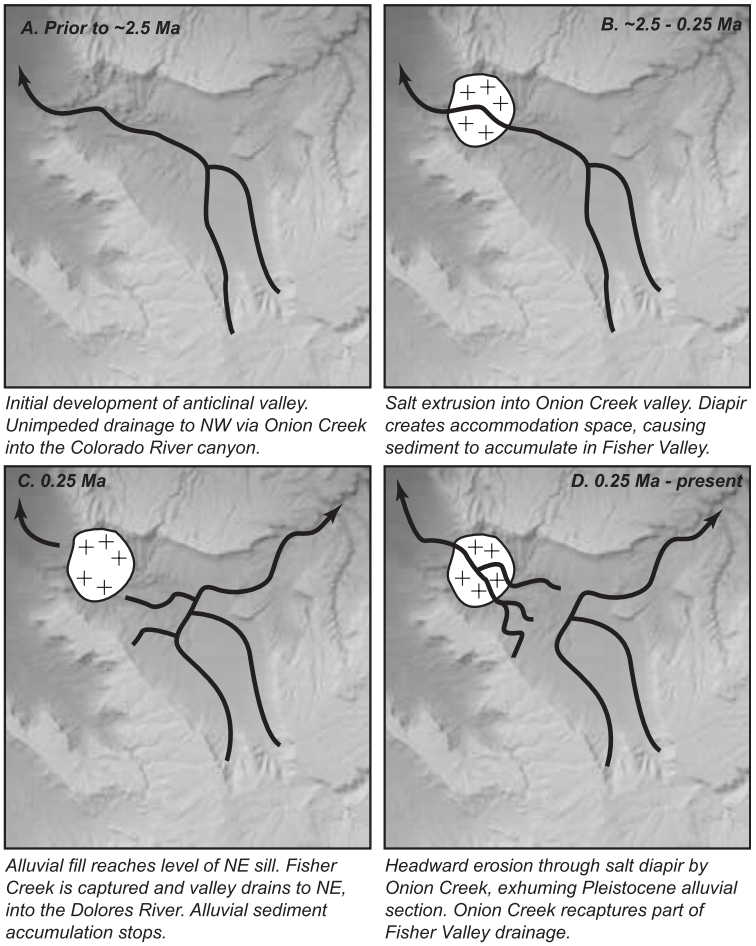

Figure 2. Geomorphic history of Fisher Valley. Colman (1983) describes the sequence of events in detail.

interglaciations) or tectonics (suggested by the evidence for episodic subsidence of the basin). The primary control on the sediment accumulation rate in the basin must have been the rate that accommodation space was created by uplift of the Onion Creek diapir. The diapir uplift rate must also have affected upstream erosion rates to some extent by controlling the local base level of Fisher Creek. However, it appears that the sediment accumulation rate was coupled to climate on the glacial–interglacial timescale. There are two possible reasons for this: erosion rates in the upstream drainage basin could have been higher during glaciations, or sediment may have been transported through the lower parts of the basin more efficiently during interglaciations, perhaps because of more effective channelization of the stream by increased vegetation cover.

Sample collection and analytical methods

In October 2000, we collected two sets of samples for cosmogenic-nuclide analysis. First, in order to establish modern erosion rates, we collected samples from (a) bedrock surfaces in the upper parts of the drainage basin, and (b) valley-bottom streams near the transition from the erosional part of the drainage basin to the depositional basin.

Second, in order to infer past erosion rates, we collected samples from the middle Pleistocene part of the alluvial section. We collected the latter samples from stratigraphic section B of Colman *et al*. (1986b) (location shown in Figure 7), which we chose because of the ease of locating the samples relative to the Lava Creek B and Bishop ashes, and because the section was located close to the lowest sample of modern stream sediment that we collected. We collected samples that were similar in age to these volcanic ashes for two reasons: first, this was the most rapidly deposited part of the section, where $N_{i,D}$ should be minimized; and second, the presence of the ashes makes this the most accurately dated part of the section. Both of these features minimize the effect of uncertainties in the sediment

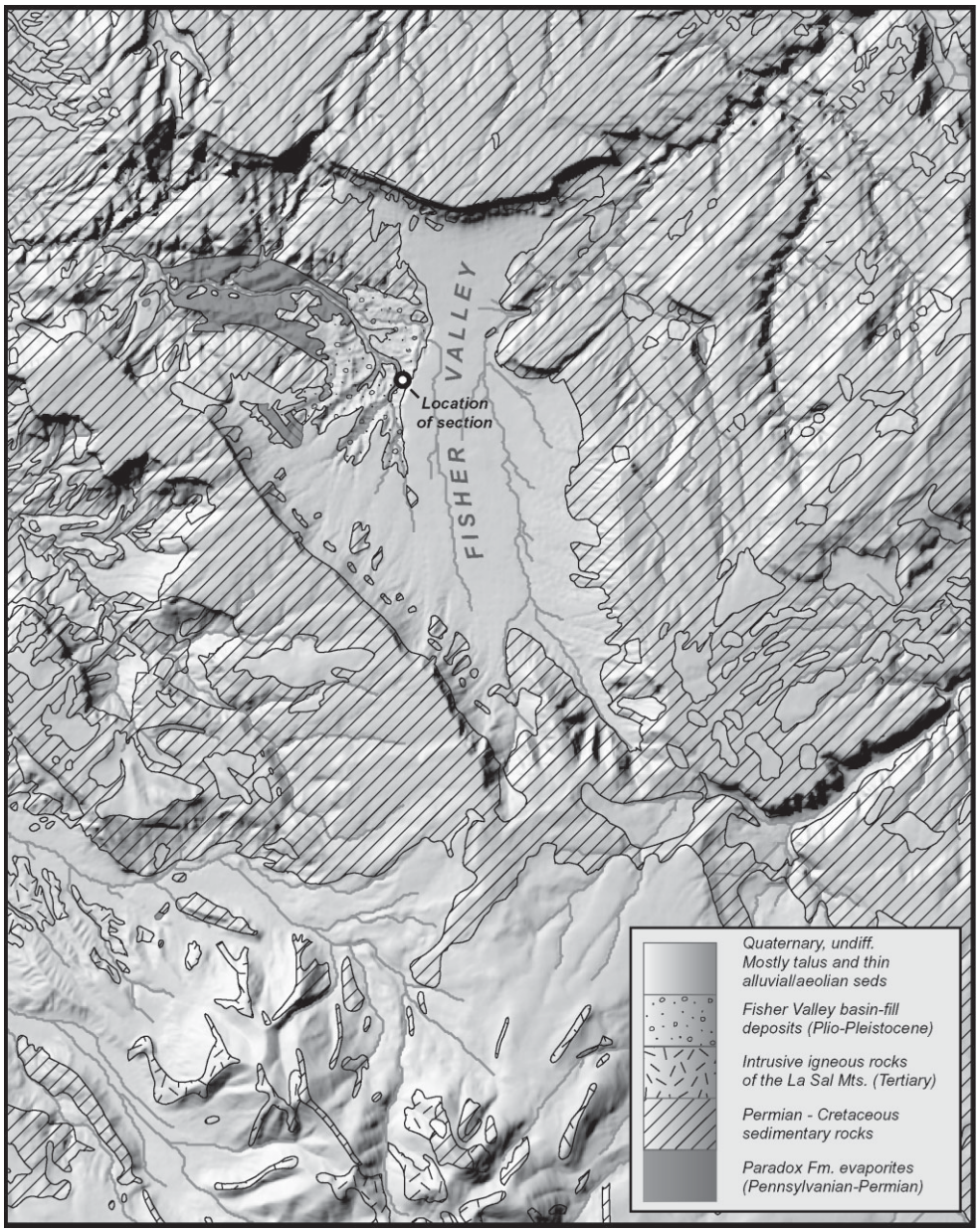

Figure 3. Geological map of Fisher Valley. Data from Doelling (2002).

age model. At present, there is essentially complete exposure of the alluvial section on steep, barren, and rapidly eroding slopes at the headwaters of Onion Creek (Figure 4). We collected the samples by identifying the horizon we wished to sample on the surface of the outcrop, then moving uphill a measured distance and using a hand auger to sample the unit of interest at 2·5 m depth below the present land surface. This ensured that very little of the nuclide concentration that we measured could be attributed to re-exposure during exhumation of the section. The overall thickness of sediment removed from the lower part of the catchment during the last 0·25 Ma suggests exhumation rates of 0·2–0·5 mm a^{-1} at our sampling site; at this erosion rate and at 2·5 m depth, the ^{10}Be concentration attributable to exposure during exhumation is 2000–5000 atoms g^{-1}, which is negligible compared to measured concentrations.

We sieved the samples to the desired grain size, purified quartz by repeated etching in 2 per cent HF, extracted Al and Be by standard methods (Stone *et al*., 2004), and measured isotope ratios at the Lawrence Livermore National

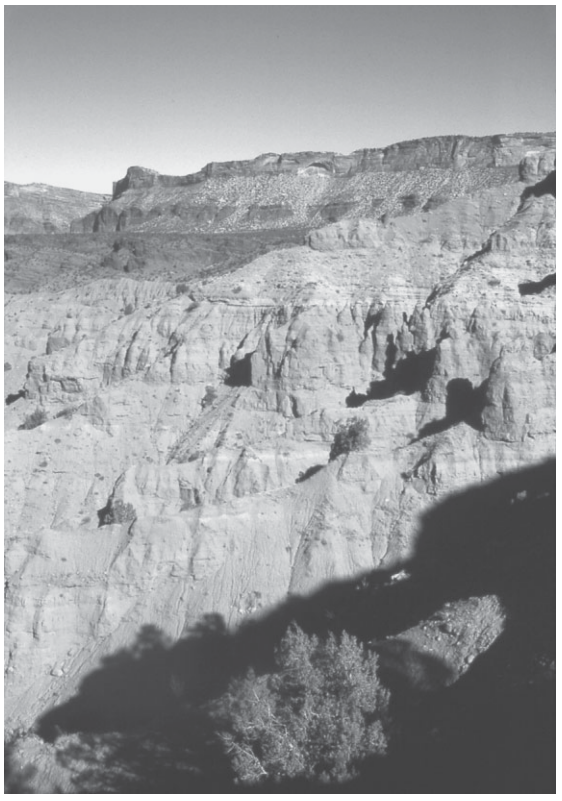

Figure 4. Pleistocene alluvial sediment at Fisher Valley, Utah, near stratigraphic section B of Colman *et al.* (1986b). The light-coloured horizons in this view are calcic palaeosols; the Lava Creek and Bishop ashes are near the bottom of the frame, but not visible in this view.

Figure 5. Headwaters of Fisher Valley. View is to the north from close to the site of bedrock sample TOP-2 (see Figure 7). Light-coloured rock at base of valley in centre of photo is the Onion Creek diapir.

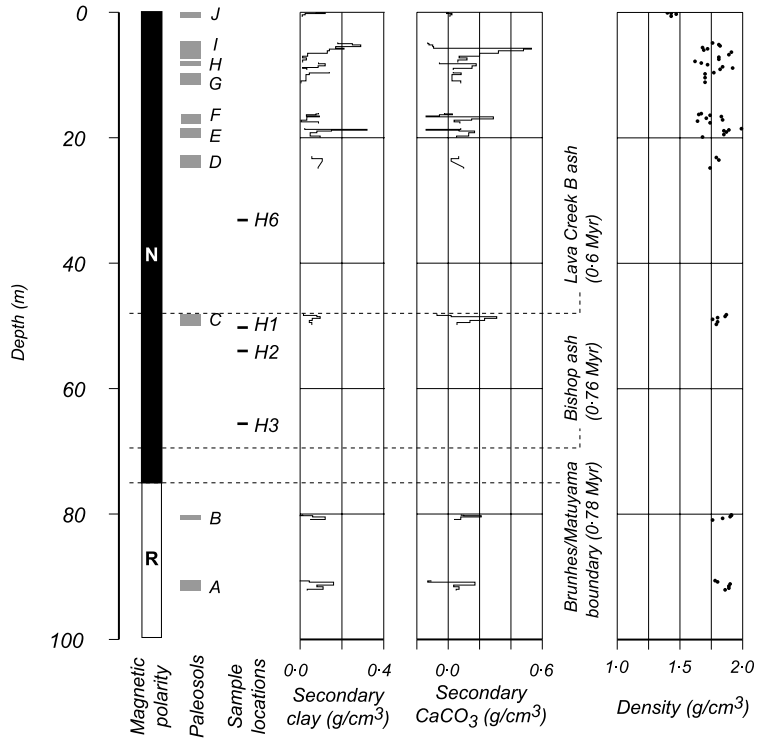

Figure 6. Stratigraphy of alluvial sediments at Fisher Valley, showing location of age control points, physical properties of palaeosols, and sample locations. This figure reproduces data from section A of Colman *et al.* (1986b). We collected samples from their section B, which is slightly thicker near the base. Thus, the depths in this figure differ slightly from those in Figure 8.

Laboratories, Center for Accelerator Mass Spectrometry (Table I). Combined process and carrier blanks were 10 000 ± 2000 atoms ^{10}Be and 65 000 ± 45 000 atoms ^{26}Al.

Data reduction methods I: inferring modern erosion rates

We used Equation 1 to calculate modern erosion rates from the nuclide concentrations in bedrock surfaces and stream sediments, with the following parameters. We used nuclide production rates from Stone (2000), and computed basin-averaged production rates by averaging production rates computed for all pixels in a 30-m digital elevation model that were within the basin. We accounted for topographic shielding of pixels, but not for production by muons or for telescoping of the effective attenuation length for spallation on steeply sloping surfaces. Balco (2001) gives details of calculating basin-averaged production rates. In this and all subsequent calculations, we assumed that the eroding material had a density of 2·5 g cm^{-3}.

Results and discussion I: modern erosion rates in Fisher Valley

Sandstone outcrops on mesas that form the upper parts of the drainage basin are eroding at 20–100 μm a^{-1} (1 μm a^{-1} = 1 m Ma) (Table II, Figure 7). These upper reaches of the basin are relatively flat and mostly soil-covered; the bedrock outcrops that are exposed above the soil surface, which we sampled, presumably represent the most slowly eroding parts of the landscape (e.g. Clapp *et al*., 2000).

Basin-averaged erosion rates inferred from medium-sand-sized quartz in streams whose drainage basins include the gently sloping uplands, a cliff band that forms the valley rim, and the gentler slopes in the lower parts of the valley, are higher, between 125 and 190 μm a^{-1} (Table II, Figure 7). Thus, it appears that erosion by retreat of steep slopes and cliffs is more effective than lowering of mesa surfaces. This is consistent with the presence of beheaded drainages on some of the mesas surrounding Fisher Valley, which suggest that drainage divides are migrating away from the valley (Colman, 1983).

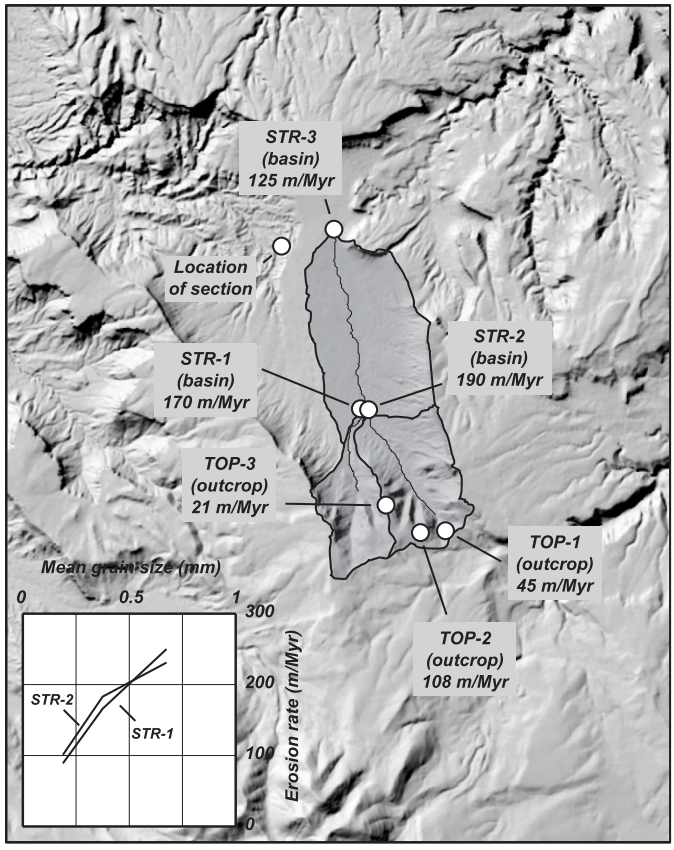

Figure 7. Modern erosion rates inferred from ^{10}Be and ^{26}Al concentrations in bedrock surfaces and stream sediment. Erosion rates inferred from bedrock samples are point measurements (Equation 1 also applies). Erosion rates inferred from stream sediments reflect the average erosion rate in the drainage basin upstream of the sample. The inset shows the relationship between sediment grain size and the inferred basin-averaged erosion rate for sample sites STR-1 and STR-2.

We also measured nuclide concentrations in different grain-size fractions in modern stream sediment, which presented a complicating factor in determining modern erosion rates. Samples of fine sand for the two sub-basins above the forks of Fisher Creek (Figure 7; sample sites STR-1 and STR-2) yielded basin-averaged erosion rates near 100 μm a^{-1}, and larger grain sizes yielded progressively higher erosion rates, approaching 250 μm a^{-1} for 0·25–0·85 mm sand (Table II, inset to Figure 7). We hypothesize that this reflects the fact that different rock types or geomorphic settings in the catchment are contributing different grain sizes to the stream sediment (e.g. Brown *et al.*, 1995; Matmon *et al.*, 2003). For example, the Wingate sandstone, which forms steep slopes, is likely eroding more rapidly than the basin as a whole, and is also probably delivering coarser sand to the stream sediment load than other rock types. The Chinle Formation, on the other hand, is largely composed of siltstone and thus both contributes finer sediment and forms lower-angle slopes that are probably eroding relatively slowly. Alternatively, it is possible that erosion rates are similar throughout the basin, but the coarse sand fraction preferentially represents rock types that form cliffs, where the local production rate is much less than in the basin as a whole due to topographic shielding effects; in this case, nuclide concentrations in the larger grain sizes would overestimate the true erosion rate unless we correctly accounted for this effect.

Both the difference in erosion rates between outcrops, sub-basins, and the entire basin, and the correlation of nuclide concentration with grain size, suggest that erosion in Fisher Valley is not spatially uniform. This is not very surprising, as the first-order geomorphology of the area makes it clear that cliff retreat outpaces overall lowering of the upland surfaces (Colman, 1983). However, it is important here because climatic or tectonic events might affect different erosional processes, and therefore erosion rates in different parts of the landscape, in different ways. For the purposes of this study, we chose to limit the effect of spatial variability in erosion rate changes, at least as expressed in the grain-size dependence of nuclide concentrations, by looking at only the 0·25–0·5 mm grain-size fraction when

Table I. Sample locations and ^{26}Al-^{10}Be concentrations

Sample name	Grain size (mm)	N Latitude	W Longitude	Elevation (m)	[^{10}Be]* (10^6 atoms g^{-1})	[^{26}Al]* (10^6 atoms g^{-1})	^{26}Al/^{10}Be ratio
Bedrock outcrops							
TOP-1	n/a	38°36′50·0″	109°11′15·9″	2527	0·459 ± 0·013	2·689 ± 0·088	5·9 ± 0·25
TOP-2	n/a	38°36′48·8″	109°11′43·9″	2580	0·202 ± 0·008	1·099 ± 0·049	5·4 ± 0·33
TOP-3	n/a	38°37′13·6″	109°12′22·3″	2592	1·022 ± 0·026	6·046 ± 0·131	5·9 ± 0·20
Modern stream sediment							
STR-1-C	0·5–0·85	38°38′38·4″	109°12′48·8″	n/a	0·069 ± 0·005	0·412 ± 0·028	6·0 ± 0·61
STR-1-M	0·25–0·5	″	″	″	0·104 ± 0·004	n.m.†	–
STR-1-F	0·125–0·25	″	″	″	0·194 ± 0·005	n.m.	–
STR-2W-C	0·5–0·85	38°38′44·4″	109°12′44·6″	″	0·068 ± 0·003	n.m.	–
STR-2W-M	0·25–0·5	″	″	″	0·085 ± 0·003	0·493 ± 0·035	5·8 ± 0·47
STR-2W-F	0·125–0·5	″	″	″	0·155 ± 0·004	n.m.	–
STR-3-M	0·25–0·5	38°41′16·5″	109°13′15·5″	″	0·116 ± 0·004	n.m.	–
Middle Pleistocene stream sediment							
H1-M	0·25–0·5	38°41′2·6″	109°14′9·2″	n/a	0·207 ± 0·006	0·892 ± 0·039	4·3 ± 0·23
H2-M	0·25–0·5	″	″	″	0·090 ± 0·003	0·383 ± 0·04	4·3 ± 0·46
H3-M	0·25–0·5	″	″	″	0·099 ± 0·004	0·393 ± 0·037	4·0 ± 0·40
H6-M	0·25–0·5	″	″	″	0·116 ± 0·006	0·446 ± 0·103	3·8 ± 0·91

* 1σ uncertainties include all known sources of analytical error. Isotope ratios are normalized to LLNL-CAMS internal standards.
† n.m. = not measured.

Table II. Modern erosion rates calculated from surface samples

	Production rates (atoms g^{-1} a^{-1})		Erosion rates (μm a^{-1})*	
Sample name	^{10}Be	^{26}Al	^{10}Be	^{26}Al
Bedrock samples† (outcrop)				
TOP-1	31·2 ± 1·9	190 ± 11	44 ± 3	45 ± 3
TOP-2	32·3 ± 1·9	197 ± 12	102 ± 7	115 ± 9
TOP-3	32·6 ± 2	198 ± 12	20 ± 1	21 ± 1
Stream sediment samples (basin-averaged)				
STR-1-C	27·1 ± 1·6	165 ± 10	250 ± 24	256 ± 23
STR-1-M	27·1 ± 1·6	165 ± 10	166 ± 11	n.m.
STR-1-F	27·1 ± 1·6	165 ± 10	89 ± 6	n.m.
STR-2W-C	24·4 ± 1·5	149 ± 9	231 ± 17	n.m.
STR-2W-M	24·4 ± 1·5	149 ± 9	183 ± 13	193 ± 18
STR-2W-F	24·4 ± 1·5	149 ± 9	101 ± 7	n.m.
STR-3-M	22·6 ± 1·4	138 ± 8	125 ± 9	n.m.

* Uncertainties in the erosion rates reflect analytical uncertainty and uncertainty in production rates from Stone (2000).
† We sawed bedrock samples to 2 cm thickness. Topographic shielding was negligible (<0·001) at the bedrock sample sites.

comparing modern and ancient samples. Thus, we may not be accurately estimating the basin-wide erosion rate, but we should accurately capture changes in the erosion rate of the parts of the basin that contribute quartz in this grain size. All erosion rates that we discuss subsequently refer to the 0·25–0·5 mm grain-size fraction.

Data reduction methods II: sediment age models, past erosion rates and uncertainty analysis

The major uncertainty in deriving past erosion rates from the nuclide concentrations in our samples of ancient alluvial sediment is that the depositional nuclide concentration $N_{i,D}$ is very sensitive to the accumulation rate of the first few

metres of sediment immediately overlying a sample. Thus, the challenge in estimating $N_{i,D}$, and thence $N_{i,E}$ and the erosion rate, is to incorporate a realistic and conservative degree of uncertainty in the sediment age model in our eventual erosion rate estimates. In our uncertainty analysis, we are mainly concerned with the new uncertainties and assumptions we introduce in inferring $N_{i,E}$ from $N_{i,M}$. The other uncertainties and assumptions related to subsequently inferring $\bar{\varepsilon}$ from $N_{i,E}$ are discussed elsewhere (Bierman and Steig, 1996; Brown *et al*., 1995; Granger *et al*., 1996; Schaller *et al*., 2004), and we do not consider them here.

We start with two conclusions drawn from previous studies of the age of the Fisher Valley section (summarized in Colman *et al*., 1986a). First, the ages of the Lava Creek and Bishop ashes are precisely known (Gansecki *et al*., 1998; van den Bogaard and Schirnick, 1995). Second, several lines of evidence indicate that the prominent palaeosols in the section formed during major interglaciations: (a) the Lava Creek ash, which was deposited immediately following a major interglaciation in marine δ^{18}O stage 15, closely overlies a prominent palaeosol; (b) the number and position of palaeosols in the stratigraphic section correspond to the number and age relationship of major interglaciations evident in marine δ^{18}O records; and (c) other relative and absolute dating methods, including thermoluminescence, U-series, and cumulative pedogenic clay and carbonate accumulations in the section, support the association of palaeosols with interglaciations (for details, see Colman *et al*., 1996a). Thus, we began constructing our sediment age model with nine age control points that consisted of pairing the measured depths of the ashes with their known ages, and pairing the measured depths of soil tops with the ages and durations of major interglaciations identified from the marine δ^{18}O record of Shackleton (1995) (Table III). We assigned a uniform 10 000-year uncertainty to the ages of the beginnings of interglaciations, a uniform 5000-year uncertainty to their durations (Table III, Figure 8), and allowed a small accumulation rate during interglaciations (uniformly distributed between 0 and 0·5 mm a^{-1}).

We then argue that: (a) the absence of additional palaeosols between these age control points indicates that there were no major (10^3–10^4 year) unrecognized breaks in sediment deposition during glacial periods; and (b), the nature of fluvial sediment accumulation suggests a high degree of variability in accumulation rates on timescales of centuries to millennia (which equates to depth scales of decimetres to metres) associated with channel migration. Following this reasoning, we used a Monte Carlo simulation to generate a large number of possible sediment age models which encapsulated both the uncertainty in the age of the control points and a high degree of shorter-timescale variability in accumulation rates. For each iteration, we began by selecting a set of age–depth control points by matching the measured depths of ashes and soil tops with ages drawn from Gaussian (for ash ages) or uniform (for ages of interglaciations picked from the δ^{18}O curve) probability distributions (Table III). We then generated a time series of accumulation rates using a first-order autoregressive model:

$$A(n+1) = 0{\cdot}95A(n) + e(n) \tag{4}$$

where $A(n)$ is the accumulation rate (arbitrary units) at step n, and $e(n)$ is a positive, normally distributed random number. We selected the weighting factor of 0·95 to produce a millennial-scale variation in accumulation rates that

Table III. Age control points used to develop randomly generated age models for the Fisher Valley section

1. *Volcanic ashes*

Ash	Depth in section (m)	Age (Ma)	Reference
Lava Creek ash	48	0·602 ± 0·002	Gansecki *et al.* (1998)
Bishop ash	82	0·760 ± 0·001	van den Bogaard and Schirnick (1995)

2. *Correlation of major interglaciations with palaeosols*

Marine δ^{18}O stage	Depth in section of soil top (m)	Age of beginning of interglaciation (Ma)	Age of end of interglaciation (Ma)
15	48·5	0·623–0·613	0·618–0·603
15	22·9	0·580–0·570	0·568–0·553
13	18·5	0·490–0·480	0·483–0·468
11	16·1	0·411–0·401	0·403–0·388
9	9·5	0·338–0·328	0·328–0·313
7	7·1	0·245–0·235	0·238–0·223
7	4·8	0·220–0·210	0·203–0·188

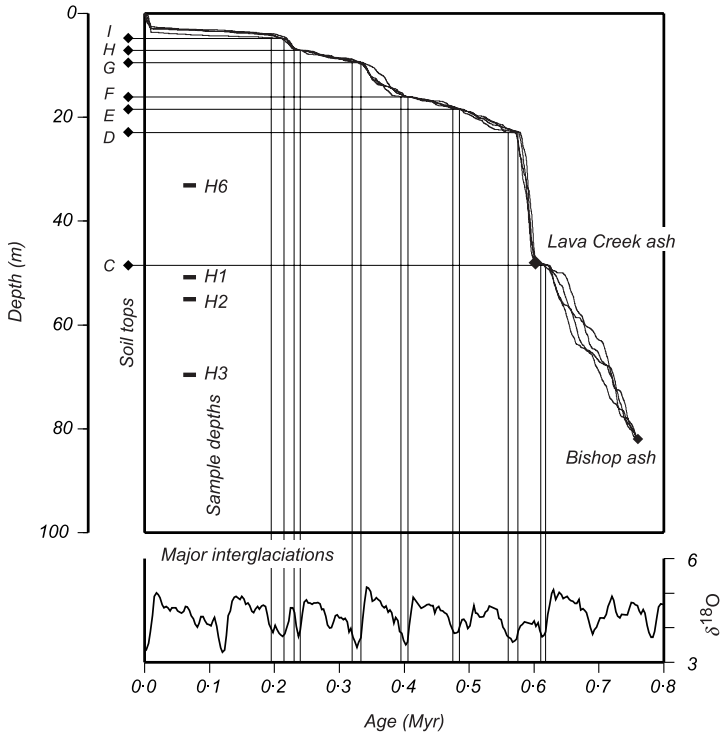

Figure 8. Age control points used to develop the randomly generated sediment age models, and examples of such age models. Filled diamonds at left show the depths of palaeosol tops. The bottom panel shows the marine $\delta^{18}O$ record used to identify major interglaciations (Shackleton, 1995). The main panel shows four examples of randomly generated age models.

would in turn yield a conservatively large range in our estimates of N_D. Finally, we assigned a time step of 100 years to this accumulation-rate time series and adjusted it (piecewise linearly) to pass through the age control points that we generated earlier. The result of this was an age model for the sediment section that was compatible with the available age constraints and with our knowledge of the depositional process (Figure 8 shows sample age models). Each of these age models yielded an age t_D for each sample.

The sediment age model provides the linear burial depth of each sample as a function of time. We then converted linear depth (m) to mass depth (g cm^{-2}) using a linear fit to the densities measured by Colman *et al*. (1986b) (see Figure 6), which resulted in the mass depth–time relationship $z(t)$.

Once armed with the function $z(t)$, we could estimate $N_{i,D}$, the nuclide concentrations produced after sediment deposition, for each sample, by solving Equation 3 for each nuclide in each sample, on the domain $t \in [0,t_D]$ where $t = 0$ at the time of sample deposition and $t = t_D$ at the present time.

The function $P_i(z)$, which is also required in Equation 3, reflects the depth dependence of nuclide production. In contrast to our simplification of Equation 1, nuclide production by muons is important in this part of the calculation. To derive $P_i(z)$, we calculated the surface production rate according to Stone (2000), assumed that production by muons follows the approximation for sea level and high latitude given in Heisinger *et al*. (2002a,b), apportioned the remainder of surface production to spallation reactions, and assumed that production by spallation reactions decreases exponentially with depth with an attenuation length Λ. The use of sea level, high latitude values for production by muons results in inaccurate production rates at moderate depths (*c*. 500–2000 g cm^{-2}), but in this particular case this uncertainty is small compared with the uncertainty in our estimate of $z(t)$. We did not consider systematic uncertainties in the calibrated nuclide production rates because, from the perspective of a particular sample, production rate uncertainties are essentially equivalent to uncertainties in sample depth, and we found that including uncertainties in production rates did not significantly affect our results.

This resulted in a range of estimates of the depositional nuclide concentrations $N_{i,D}$ for each sample, which we believe to encapsulate the largest possible degree of uncertainty that is compatible with our understanding of the age and depositional processes of the stratigraphic section. Some of the randomly generated age models resulted in

'impossible' values of $N_{i,D}$ for particular samples that exceeded the measured nuclide concentration in those samples; we discarded these age models.

We then estimated past erosion rates from each sample as follows. For each set of values for t_D, $N_{10,D}$ and $N_{26,D}$ derived from a particular age model, we chose randomly generated values for the measured nuclide concentrations in each sample from a Gaussian probability distribution centred on the actual measurement and reflecting the analytical uncertainty. At this point, we had two measurements ($N_{26,M}$ and $N_{10,M}$) which must reflect a single erosion rate $\bar{\varepsilon}$. We used standard optimization methods to choose the value of $\bar{\varepsilon}$ that minimized the chi-squared difference between the measured nuclide concentrations predicted by Equations 1 and 2, and the values of $N_{i,M}$ chosen in each iteration. In applying Equation 1, we used the basin-averaged production rate that we computed for our lowest sample of modern stream sediment (STR-3; see Table II and Figure 7).

Results and discussion II: past erosion rates in Fisher Valley

Erosion rates in Fisher Valley between 0·7 and 0·58 Ma most likely varied between 80 and 220 μm a^{-1} (Figure 9, Table IV). We found that we could confidently exclude erosion rates lower than the most likely values, but were not able to categorically exclude much higher erosion rates in the past. This effect is most pronounced for the stratigraphically lowest pair of samples (H2-M and H3-M). These samples have low measured nuclide concentrations, which are similar to the predicted values of the depositional nuclide concentrations $N_{i,D}$: thus, we are in effect deriving $N_{i,E}$ by subtracting two large and uncertain numbers from each other, which enhances the relative uncertainty in the resulting small number. The inverse relationship between $N_{i,E}$ and $\bar{\varepsilon}$ in Equation 1, which causes the uncertainty in $\bar{\varepsilon}$ to be large when $N_{i,E}$ is small, then results in a very large uncertainty in the erosion rates. In the case of the upper pair of samples, this effect is less pronounced and the past erosion rates are better constrained.

Even though the erosion rates inferred from the lowest two samples (180–220 μm a^{-1}) are relatively uncertain, they are significantly higher than those inferred from the upper two samples (80–120 μm a^{-1}). Although we cannot

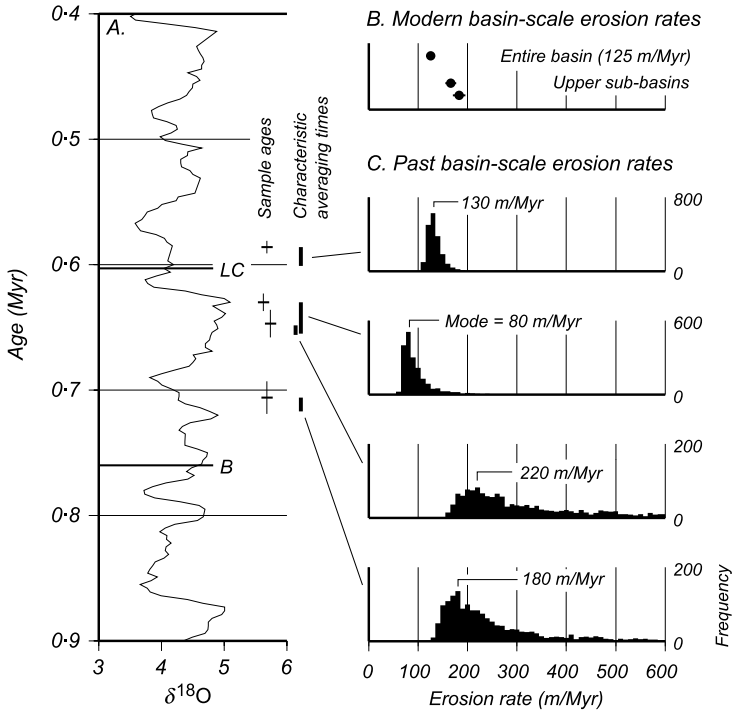

Figure 9. Past basin-scale erosion rates inferred from buried alluvial sediment samples, and their relationship to glacial–interglacial climate changes. (A) Marine benthic $\delta^{18}O$ record from Shackleton (1995). Crosses show mean and 1σ error of sample ages inferred from Monte Carlo simulation described in the text. Dark bars indicate characteristic averaging time associated with the erosion rates inferred from sediment samples. (B) Modern basin-scale erosion rates (duplicating the data in Figure 7). (C) Results of error analysis of past erosion rate measurements. Histograms show results of 2000-point Monte Carlo simulation described in the text. The modal erosion rate is indicated on the diagram and is also the value reported in Table IV.

Table IV. Past erosion rates inferred from buried sediment

Sample name	Depth in section (m)	Age (Ma)*	Most likely erosion rate (μm a^{-1})
H6-M	33·1	0·586 ± 0·005	130
H1-M	50·8	0·630 ± 0·007	80
H2-M	55·0	0·647 ± 0·011	220
H3-M	69·6	0·706 ± 0·013	180

* Estimated from Monte Carlo simulation described in text.

adequately evaluate the relationship between glacial–interglacial climate change and erosion rates using only these four measurements, both relatively high and relatively low erosion rates occur during glacial periods, providing no evidence of any such relationship. On the other hand, one of the angular unconformities near the edges of the Fisher Valley alluvial section is stratigraphically between the Lava Creek and Bishop ashes (Colman *et al*., 1986b). The association of relatively high erosion rates (compared to those of 0·63–0·59 Ma and at the present time) with evidence of unusually rapid deformation suggests that the change in erosion rates was most likely the result of tectonic activity rather than climate change.

Summary and Conclusions

Past erosion rate changes in Fisher Valley

Although we have only a few data, which are not enough to convincingly answer the question of whether erosion rates in Fisher Valley responded to climate changes, tectonic events, or both, we make the following conclusions.

1. Erosion rates in Fisher Valley at 0·7–0·6 Ma were broadly similar to the present erosion rate, but varied by a factor of two or more during that time.
2. Both relatively high and low erosion rates occurred during glacial periods. Therefore, there is no compelling evidence for any relationship between glacial–interglacial climate change and erosion rates. On the other hand, relatively high erosion rates at 0·7–0·65 Ma were approximately coeval with an episode of unusually rapid subsidence or deformation, suggesting a relationship between tectonic activity, perhaps expressed as base-level change or oversteepening of valley walls, and erosion rates.
3. Both relatively high and relatively low basin-wide erosion rates occurred during periods when the sediment accumulation rate was relatively high (Figure 8). This indicates that the trapping efficiency of the basin was changing through time, and highlights the fact that sediment production and sediment accumulation almost certainly responded in different ways to changes in the climatic or tectonic environment.

Strengths and weaknesses of our approach

The approach of measuring past erosion rate changes by cosmogenic-nuclide concentrations in ancient alluvial sediment improves on mass-balance methods of measuring past erosion rate changes by requiring only a small sample, and not the entire inventory, of sediment shed from the eroding landscape at a particular time. It can improve on thermochronologic methods of reconstructing past exhumation rates because the short depth scale of cosmogenic-nuclide accumulation equates to an ability to resolve much more rapid erosion rate changes than possible with thermochronology. Our emphasis on continually deposited alluvial sediment sections in this paper is, in principle, a potential improvement on previous studies that inferred past basin-scale erosion rates from cosmogenic-nuclide concentrations in ancient sediment because those studies focused on episodically deposited sedimentary records, that is, river terraces and cave sediments, which only record certain types of climatic or hydrological transitions and thus provide a very restricted sample of the time variability of erosion rates.

On the other hand, the idea of extracting continuous records of past erosion rates from subaerial sedimentary sections is subject to new uncertainties which potentially limit its usefulness. In particular, we show in this paper that the need to estimate $N_{i,D}$ from an imperfectly dated stratigraphic section results in a large uncertainty in measuring past erosion rates. The major weakness in our example from Fisher Valley is our procedure of estimating the uncertainty in

$N_{i,D}$ from a large number of randomly generated age models. As our age control points are separated by metres to tens of metres, we cannot use them directly to create an age model accurate enough to determine $N_{i,D}$ with any certainty, and we must focus more on a conservative estimate of the uncertainty in $N_{i,D}$ than on its actual value. In carrying out the uncertainty analysis, in turn, we have only weak stratigraphic or sedimentological grounds for asserting that each of our randomly generated age models has equal likelihood, an assertion which is necessary if we are to interpret the resulting distributions of possible past erosion rates as probability distributions.

We could solve this problem of estimating $N_{i,D}$ in three ways. First, we could improve the geological part of our study, that is, we could better constrain the sediment age model by looking at the stratigraphy of the fluvial deposits in enough detail to identify fining-upward packages, channel abandonment events, small-scale unconformities, or other evidence that would tell us about the decimetre- to metre-scale variation in sediment accumulation rates that controls $N_{i,D}$. Second, we could look for geochemical or sedimentological proxies for sediment accumulation rates, for example, magnetic susceptibility, secondary clay content, or soil carbonate accumulation (e.g. Anderson and Hallet, 1996), that would enable us to better understand small-scale variations in sediment accumulation without the need for unrealistically accurate absolute dating of each horizon. Third, we could better plan our sampling strategy to exploit the fact that the nuclide concentration due to erosion $N_{i,E}$ integrates 5000–10 000 years of erosion, so must be similar in adjacent packages of sediment, but the depositional nuclide concentration $N_{i,D}$ may be very different in adjacent samples because it reflects potentially large and rapid decimetre-scale variations in accumulation rates. Thus, with spatially dense sampling, we could in principle use the contrast between high- and low-frequency variability in measured nuclide concentrations to separate variability in $N_{i,D}$ from that in $N_{i,E}$. To summarize, although the record of past erosion rates in Fisher Valley that we use as an example here is not yet precise enough or detailed enough to provide satisfying answers to the question of how erosion rates in the basin relate to climatic or tectonic events, we could in principle answer this question by improving both our stratigraphic observations and our sampling strategy.

Finally, we discuss the larger question of how we might best use the idea of reconstructing erosion rates from cosmogenic-nuclide concentrations in ancient sediment to answer questions about the relationship of climate, tectonics, and erosion in other geological settings. The most important observation in this context is that most of the complications that arise in inferring past erosion rates from present nuclide concentrations disappear if $N_{i,D} = 0$, that is, if the sediment is deposited in deep water. Thus, we emphasize again that this technique will be most accurate, and therefore most useful, when applied to deep-water sediments. The goal of obtaining long sections of detrital quartz sand from marine or lacustrine sediments does present new problems, including the need to understand sediment transport paths in detail, the expense of collecting sediment cores in deep water, and the difficulty of obtaining large samples of sand-sized quartz from sediment cores. However, the potential improvements in understanding the coupled climate–erosion–tectonics system that could result from continuous, relatively high-resolution records of past erosion rates justifies an effort to incorporate this goal in future shallow-marine and lacustrine drilling programmes.

Acknowledgements

Greg Balco was supported by a graduate fellowship from the Fannie and John Hertz Foundation, grants from the American Federation of Mineralogical Societies and DOSECC, and the Mackin Award of the Geological Society of America. Marc Caffee of the Center for Accelerator Mass Spectrometry, Lawrence Livermore National Laboratory, was instrumental in the AMS analyses. We appreciate constructive reviews by Greg Hancock and Paul Bierman.

References

Anderson RS, Hallet B. 1996. Simulating magnetic susceptibility profiles in loess as an aid in quantifying rates of dust deposition and pedogenic development. *Quaternary Research* **45**: 1–16.

Balco G. 2001. Topographic shielding and cosmogenic nuclide production rates over large areas. http://depts.washington.edu/cosmolab/math.html

Bierman PR, Steig E. 1996. Estimating rates of denudation using cosmogenic isotope abundances in sediment. *Earth Surface Processes and Landforms* **21**: 125–139.

Bierman PR, Nichols KK. 2004. Rock to Sediment – Slope to Sea with ^{10}Be – Rates of Lanscape Change. *Annual Review of Earth and Planetary Sciences* **32**: 215–255.

Brown ET, Stallard RF, Larsen MC, Raisbeck GM, Yiou F. 1995. Denudation rates determined from the accumulation of in situ-produced ^{10}Be in the Luquillo Experimental Forest, Puerto Rico. *Earth and Planetary Science Letters* **129**: 193–202.

Cerling TE, Craig H. 1994. Geomorphology and in-situ cosmogenic isotopes. *Annual Review of Earth and Planetary Sciences* **22**: 273–317.

Clapp EM, Bierman PR, Schick AP, Lekach J, Enzel Y, Caffee M. 2000. Sediment yield exceeds sediment production in arid region drainage basins. *Geology* **28**: 995–998.

Collier REL, Leeder MR, Trout M. 2000. High sediment yields and cool, wet winters: Test of last glacial paleoclimates in the northern Mediterranean. *Geology* **28**: 999–1002.

Colman SM. 1983. Influence of the Onion Creek salt diapir on the late Cenozoic history of Fisher Valley, Utah. *Geology* **11**: 240–243.

Colman SM, Hawkins FF. 1985. *Surficial geologic map of the Fisher Valley-Professor Valley area, southeastern Utah*. US Geological Survey Miscellaneous Investigations Series, Map I-1596.

Colman SM, Choquette AF, Rosholt JM, Miller GH, Huntley DJ. 1986a. Dating the upper Cenozoic sediments in Fisher Valley, Utah. *Geological Society of America Bulletin* **97**: 1422–1431.

Colman SM, Choquette AF, Hawkins FF. 1986b. *Physical, soil, and paleomagnetic stratigraphy of the upper Cenozoic sediment in Fisher Valley, southeastern Utah*. US Geological Survey Bulletin 1686.

Doelling HH. 2002. *Geologic map of the Moab and the eastern part of the San Rafael Desert 30′ × 60′ quadrangles*. Utah Geological Survey Map 180DM.

Gansecki CA, Mahood GA, McWilliams M. 1998. New ages for the climactic eruptions at Yellowstone: single-crystal $^{40}Ar/^{39}Ar$ dating identifies contamination. *Geology* **26**: 343–346.

Garver JI, Brandon MT, Roden-Tice MK, Kamp, PJJ. 1999. Exhumation history of orogenic highlands determined by detrital fission-track thermochronology. In *Exhumation Processes: Normal Faulting, Ductile Flow, and Erosion*, Ring U, Brandon MT, Lister GS, Willett SD (eds). Special Publications 154. Geological Society: London; 283–304. Geological Society.

Granger DE, Kirchner JW, Finkel RC. 1996. Spatially averaged long-term erosion rates measured from in-situ-produced cosmogenic nuclides in alluvial sediment. *Journal of Geology* **104**: 249–257.

Granger DE, Kirchner JW, Finkel RC. 1997. Quaternary downcutting rate of the New River, Virginia, measured from differential decay of cosmogenic ^{26}Al and ^{10}Be in cave-deposited alluvium. *Geology* **25**: 107–110.

Granger DE, Fabel D, Palmer AN. 2001. Pliocene–Pleistocene incision of the Green River, Kentucky, determined from radioactive decay of cosmogenic ^{26}Al and ^{10}Be in Mammoth Cave sediments. *Geological Society of America Bulletin* **113**: 825–836.

Heisinger B, Lal D, Jull AJT, Kubik P, Ivy-Ochs S, Neumaier S, Knie K, Lazarev V, Nolte E. 2002a. Production of selected cosmogenic radionuclides by muons 1. Fast muons. *Earth and Planetary Science Letters* **200**: 345–355.

Heisinger B, Lal D, Jull AJT, Kubik P, Ivy-Ochs S, Knie K, Nolte E. 2002b. Production of selected cosmogenic radionuclides by muons 2. Capture of negative muons. *Earth and Planetary Science Letters* **200**: 357–369.

Koppes MN, Hallet B. 2002. Influence of rapid glacial retreat on the rate of erosion by tidewater glaciers. *Geology* **30**: 47–50.

Lal D. 1991. Cosmic-ray labeling of erosion surfaces: in situ nuclide production rates and erosion models. *Earth and Planetary Science Letters* **104**: 424–439.

Langbein WB, Schumm SA. 1958. Yield of sediment in relation to mean annual precipitation. *Transactions, American Geophysical Union* **39**: 1076–1084.

Matmon A, Bierman PR, Larsen J, Southworth S, Pavich M, Finkel R, Caffee M. 2003. Erosion of an ancient mountain range, the Great Smoky Mountains, North Carolina and Tennessee. *American Journal of Science* **303**: 817–855.

Molnar P. 2003. Geomorphology: Nature, nurture, and landscape. *Nature* **426**: 612–614.

Molnar P, England J. 1990. Late Cenozoic uplift of mountain ranges and global climate change: chicken or egg? *Nature* **346**: 29–34.

Nishiizumi K, Winterer EL, Kohl CP, Klein J, Middleton R, Lal D, Arnold JR. 1989. Cosmic ray production rates of ^{26}Al and ^{10}Be in quartz from glacially polished rocks. *Journal of Geophysical Research*, **94**: 17907–17915.

Pazzaglia FJ, Brandon MT. 1996. Macrogeomorphic evolution of the post-Triassic Appalachians determined by de-convolution of the offshore marine sedimentary record. *Basin Research* **8**: 255–278.

Raymo ME, Ruddiman WF. 1992. Tectonic forcing of late Cenozoic climate. *Nature* **359**: 117–122.

Reiners PW, Ehlers TA, Mitchell SG, Montgomery DR. 2003. Coupled spatial variations in precipitation and long-term erosion rates across the Washington Cascades. *Nature* **426**: 645–647.

Riebe CS, Kirchner JW, Granger DE, Finkel RC. 2001. Minimal climatic control on erosion rates in the Sierra Nevada, California. *Geology* **29**: 447–450.

Schaller M, von Blanckenburg F, Veldkamp A, Tebbens LA, Hovius N, Kubik PW. 2002. A 30 000 yr record of erosion rates from cosmogenic ^{10}Be in Middle European river terraces. *Earth and Planetary Science Letters* **204**: 307–320.

Schaller M, von Blanckenburg F, Hovius N, Veldkamp A, van den Berg MW, Kubik PW. 2004. Paleoerosion rates from cosmogenic ^{10}Be in a 1.3 Ma terrace sequence: response of the river Meuse to changes in climate and rock uplift. *Journal of Geology* **112**: 127–144.

Schumm SA, Hadley RF. 1961. *Progress in the application of landform analysis in studies of semiarid erosion*. US Geological Survey Circular 437.

Schumm SA, Rea DK. 1995. Sediment yield from disturbed earth systems. *Geology* **23**: 391–394.

Shackleton N. 1995. New data on the evolution of Pliocene climate variability. In *Paleoclimate and Evolution, with Emphasis on Human Origins*, Vrba E, Denton GH, Partridge TC, Burckle LC (eds). Yale: New Haven; 242–248.

Shoemaker EM. 1954. Structural features of southeastern Utah and adjacent parts of Colorado, New Mexico, and Arizona. In *Guidebook to the Geology of Utah*, Stokes WL (ed.). Utah Geological Society Guidebook No. 9: 44–69.

Stone JO. 2000. Air pressure and cosmogenic isotope production. *Journal of Geophysical Research* **105**: 23753–23759.

Stone JOH, Todd C, Balco G. 2004. Extraction of Al and Be from quartz for isotopic analysis. University of Washington Cosmogenic Isotope Lab, Methods and Procedures. http://depts.washington.edu/cosmolab/chem.html

van den Bogaard P, Schirnick C. 1995. $^{40}Ar/^{39}Ar$ laser probe ages of Bishop Tuff quartz phenocrysts substantiate long-lived silicic magma chamber at Long Valley, United States. *Geology* **23**: 759–762.

